Environ Monit Assess (2019) 191: 235
https://doi.org/10.1007/s10661-019-7355-x

An automatic water detection approach using Landsat 8 OLI and Google Earth Engine cloud computing to map lakes and reservoirs in New Zealand

Uyen N. T. Nguyen · Lien T. H. Pham · Thanh Duc Dang

Received: 19 July 2018 / Accepted: 1 March 2019 / Published online: 21 March 2019
© Springer Nature Switzerland AG 2019

Abstract Monitoring water surface dynamics is essential for the management of lakes and reservoirs, especially those are intensively impacted by human exploitation and climatic variation. Although modern satellites have provided a superior solution over traditional methods in monitoring water surfaces, manually downloading and processing imagery associated with large study areas or long-time scales are time-consuming. The Google Earth Engine (GEE) platform provides a promising solution for this type of "big data" problems when it is combined with the automatic water extraction index (AWEI) to delineate multi-temporal water pixels from other forms of land use/land cover. The aim of this study is to assess the performance of a completely automatic water extraction framework by combining AWEI, GEE, and Landsat 8 OLI data over the period 2014–2018 in the case study of New Zealand. The overall accuracy (OA) of 0.85 proved the good performance of this combination. Therefore, the framework developed in this research can be used for lake and reservoir monitoring and assessment in the future. We also found that despite the temporal variability of climate during the period 2014–2018, the spatial areas of most of the lakes (3840) in the country remained the same at around 3742 km^2. Image fusion or aerial photos can be employed to check the areal variation of the lakes at a finer scale.

Keywords Automatic water extraction index · Google Earth Engine · Water surface · New Zealand · Landsat 8 OLI

U. N. T. Nguyen (✉)
Environmental Research Institute, The University of Waikato, Hamilton, New Zealand
e-mail: uyenn@email.arizona.edu

L. T. H. Pham
HCMC University of Science, Vietnam National University, Ho Chi Minh City, Vietnam

T. D. Dang
Institute for Water and Environment Research, Thuy Loi University, Ho Chi Minh City, Vietnam

Introduction

Modifications to surface water dynamics can result in alterations to lentic and lotic water cycles (Wood et al. 2011). Monitoring is extremely important since any modifications can alter water quality and quantity, water availability, and the functional and physical processes of ecosystem (Cann et al. 2013; Dang et al. 2016). It is, therefore, important to have an accurate and precise water surface mapping method to improve large-scale water management. Before the remote sensing era, the ground survey was the only method available. While this traditional method was costly and time-consuming, results were not always spatially accurate. Remote sensing provides a spatial and temporal technique capable of tracing a historical record; therefore, it is useful for monitoring lake information over a time period in areas not having a ground-based monitoring program. There were extensive efforts to monitor the dynamics of water surface by remote sensing, for example, McCullough

et al. (2013), Feyisa et al. (2014), Gao et al. (2014), or Fisher et al. (2016). Remote sensing was also applied to help the assessment and management of water quality, flood hazard, and damage identification, as well as changes in surface water resources (Proud et al. 2011; Prigent et al. 2012; Güttler et al. 2013; Dang et al. 2016; Dang et al. 2018b). This technique can act as an essential resource for policy- and decision-makers on local, regional, and national scales (Giardino et al. 2010, Nguyen et al. 2015, Nguyen 2015). However, most of the existing studies were either implemented for a small study area (i.e., 70 × 22 km in Proud et al. 2011) or a short period of time (i.e., 2 years as in Dang et al. 2018b). This was caused by the time-consuming problem of the data downloading and processing procedures.

Different water indices (e.g., normalized difference water index (NDWI), modified normalized difference water index (MNDWI), water index 2006 (WI_{2006}), and water index 2015 (WI_{2015})) can be adopted to obtain information accurately and quickly (Ouma and Tateishi 2006; Bai et al. 2011; Qiao et al. 2012; Li et al. 2013; Feyisa et al. 2014). Manual classifications based on satellite images are reliant on human expertise, and, therefore, result in relatively slow and subjective to bias due to misinterpretation. For optical imagery, water classification methods use one or a combination of techniques which include single-band thresholding, linear unmixing, two-band spectral water indices, and thematic classification (Ji et al. 2009; Sun et al. 2012; Pham and Brabyn 2017; Dang et al. 2018b). Different indices (e.g., NDWI, MNDWI, WI_{2006}, and WI_{2015}) were employed to mask water from other types of land use/land cover (Pham et al. 2019; Nguyen et al. 2019). Originally developed by McFeeters (1996), NDWI is a relatively simple index using the input of two bands. However, the difficulty of this index is to accurately discriminate between water pixels and built-up areas. This led to the invention of MNDWI which substituted the middle-infrared band for the near-infrared band of Landsat 5 TM (Xu 2006). MNDWI was used to map surface water, land use change, and other ecological applications (Hui et al. 2008; Duan and Bastiaanssen 2013). Another water index was WI_{2006} combining five bands and enabling the masking of water pixels (Danaher and Collett 2006). This was later updated by Fisher et al. (2016)—using the WI_{2015} index. With all these indices, a threshold is chosen whereby water pixels are classified.

These water classification techniques using the mentioned indices may contain uncertainties and reduce the accuracy in areas where surrounding land covers are dominated by asphalt roads, shadows, and other low albedo surfaces (Xu 2006; Verpoorter et al. 2012). This misclassification occurred because of the similarity of reflectance between these land cover pixels and water pixels. The misclassification was also found when single or two-band threshold approaches were used to distinguish between water pixels and non-water dark surfaces. Therefore, Feyisa et al. (2014) proposed the automatic water extraction indices (AWEI), which combined more than two spectral bands for the improvement of water surface identification. AWEI includes two types: an index for images without shadow ($AWEI_{no\ shadow}$) and an index for images with shadow from mountains, clouds, or other objects ($AWEI_{shadow}$) using four and five bands respectively. The AWEI indices were then applied in several case studies related to water surface classification, and the overall accuracy (OA) values were high (OA > 0.93) (Feyisa et al. 2014; Feng et al. 2016; Fisher et al. 2016). In addition to high percentage accuracy, only minor amounts of variation were observed in optimum AWEI thresholds when the AWEI index was derived from surface reflectance images (Feyisa et al. 2014). This may consequently allow the advancement of large-scale automated mappings of land surface water, such as lake surfaces on a national scale, instead of focusing on a specific location or sensor. These studies, however, only focused on spatial distributions of water surface at certain times. Intermittent monitoring might result in misclassification because several kinds of water surfaces which only appeared in a certain area at a certain time. As a result, automatic multi-temporal water surface detection is needed.

Google Earth Engine is a cloud-based platform, which can be used to execute large-scale and long-term geospatial analysis (Gorelick et al. 2017). This public-domain platform utilizes the computational capacities of Google Servers, so it allows us to advance our capabilities in earth exploration. This cloud computing platform has been applied in crop classification and water extraction. Donchyts et al. (2016), Shelestov et al. (2017), and Feng et al. (2016), however, used the single- or two-band threshold approaches which might cause

errors in automatic water extraction processes as aforementioned.

The primary objective of this study is to examine the use of combined AWEI and GEE in automating water surface extraction for large-scale and long-term monitoring purposes. New Zealand was chosen as a case study because this was an agriculture-based country with large areas covered by water and accurate up-to-date mapping is critical to its distinct biodiversity and agricultural productivity.

Study area

In the center of the southern hemisphere, New Zealand (location in Fig. 1) includes two main islands, the North and South Islands. New Zealand is an agriculture/forestry-based exporter, including dairy, wood, fruits, and other animal-related products (New Zealand statistics 2006). Because of its geographical isolation, the country developes a unique biodiversity of flora and fauna. Lake and reservoir management, therefore, plays

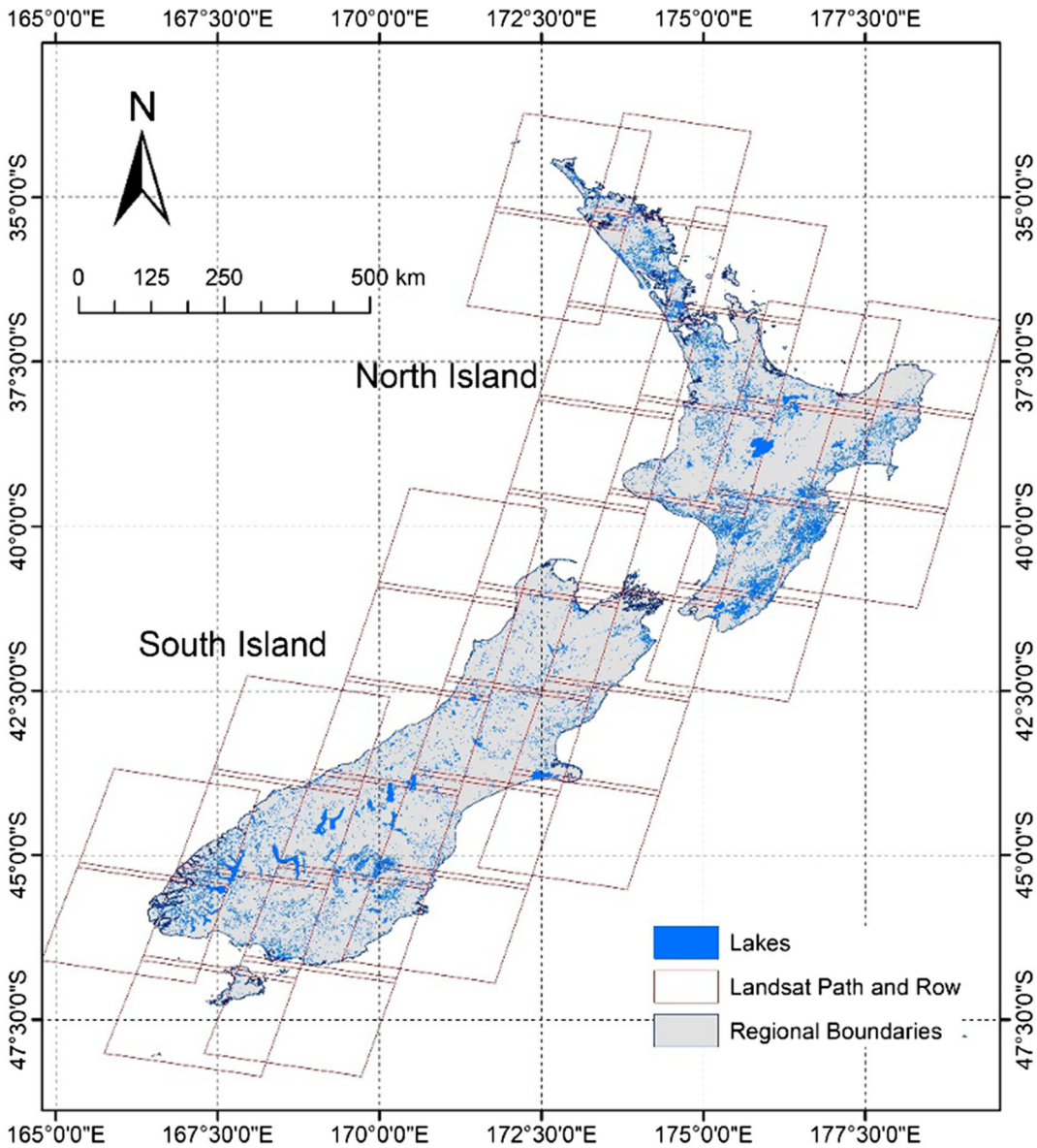

Fig. 1 Map of New Zealand, Landsat path and row, and lakes

a crucial role in its economic development and biodiversity conservation.

New Zealand is located in a long and narrow region along the north-south axis, which makes its climate temperate maritime. Generally, the snow season lasts from early June to early October in the eastern and southern parts of the South Island and mountainous regions.

New Zealand was, however, chosen to implement this study not only because of the importance of water dynamic monitoring to its ecological diversity and agricultural productivity but also because of its diverse lake system, ranging from glacial to volcanic lakes and from shallow to deep lakes. Lowe and Green (1992), via field surveys, listed various types of lakes in their research such as tectonic, volcanic, glacier, artificial, peat, solution, barrier-bar, landslide, or riverine lakes. For example, Rotorua lakes in the Bay of Plenty area include very deep lakes such as Lake Tarawera, Lake Rotoiti, and Lake Rotoma which have complex characteristics in terms of water quality. Lake Tekapo and Pukaki in the middle South Island, for example, have milky-turquoise color from the fine rock-flour originated from glacial ranges and suspended in water. There is also phytoplankton on blue-green algal bloom lakes, for example, Lake Rotoehu (alga), Lake Okareka, and Lake Ngaroto (aquatic vegetation). Figure 2 illustrates the difference in water characteristics of lakes in New Zealand. This complexity may be translated into errors in water surface extraction if a proper classification method was not chosen.

Materials and methodology

Landsat 8 OLI acquisition

Although there were several satellite products varying in spatial, temporal, and spectral characteristics (e.g., MODIS, SPOT, or Sentinel), Landsat was used for this study. Advantages of Landsat imagery are its free availability, and temporal (16 days) and spatial resolutions (30 m). Landsat sensors can spatially interpret lakes with a resolution of 30 m with 16-day orbit to the same site. Additionally, Landsat was one of the first remote sensing imagery services (1972).

The advantages of Landsat 8 OLI over previous versions such as Landsat 7 include improving radiometric resolution and reducing image noise and spectral heterogeneity, which provides a more precise water

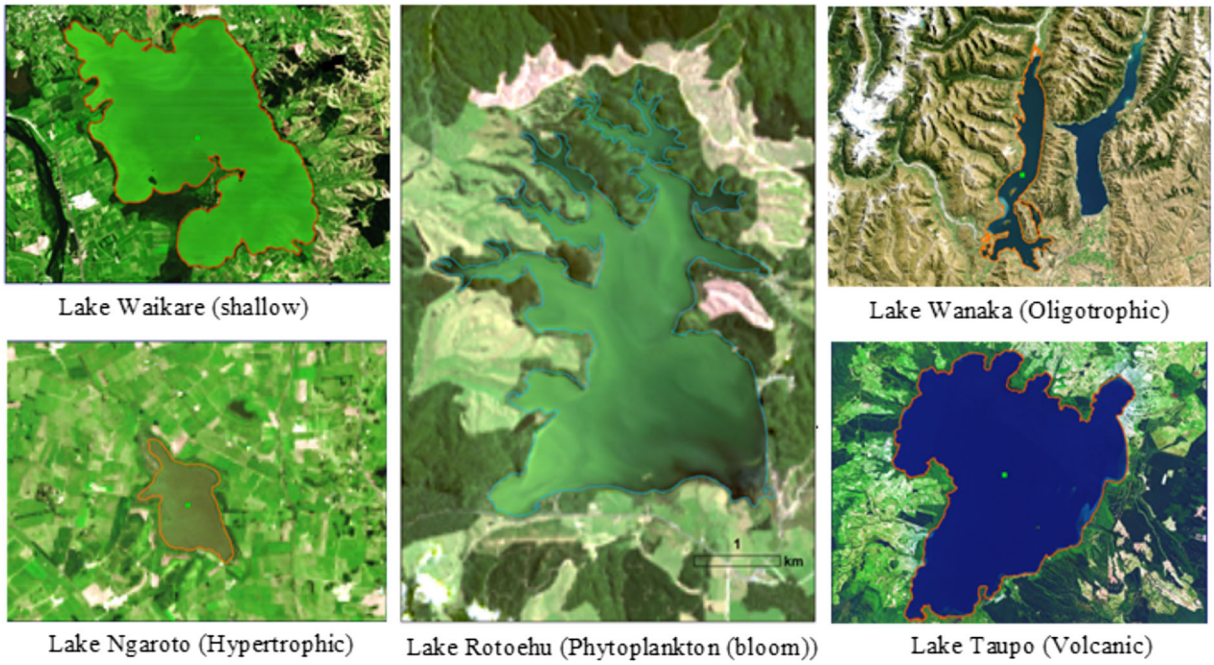

Fig. 2 Lake and reservoir boundaries with different sizes and water characteristics generated from Landsat 8 images in natural colors. Among of them, eutrophic lakes are enriched with nutrients associated with land use; oligotrophic lakes, having low concentration of vegetation, are found in glacier mountains; NZ has a lot of active volcanoes and volcanic lakes

surface extraction and water quality retrievals (Lymburner et al. 2016). The OLI sensor collects data in nine shortwave bands: eight spectral bands at 30-m resolution and one panchromatic band at 15 m. OLI data products have a 16-bit range, narrow spectral bands.

In this study, we mapped the water surface of lakes and reservoirs with Landsat 8 OLI records of the period from 2013 to 2017. Landsat 8 OLI data archived from pre-collection from USGS Earth Resources Observation and Science (EROS) Center Science Processing Architecture (ESPA) on demand interface (https://eros.usgs.gov/). Surface reflectance Tier 1 products of Landsat can be also queried, visualized, and analyzed on Google Earth Engine (GEE). Approximately 498 scenes with free-cloud imagery were acquired with corrections for atmospheric scattering and aerosol absorptions by using Landsat 8 Surface Reflectance Code (LarSRC), including masking of clouds, shadows, and per-pixel saturation (https://code.earthengine.google.com/dataset/LANDSAT/LC08/C01/T1_SR).

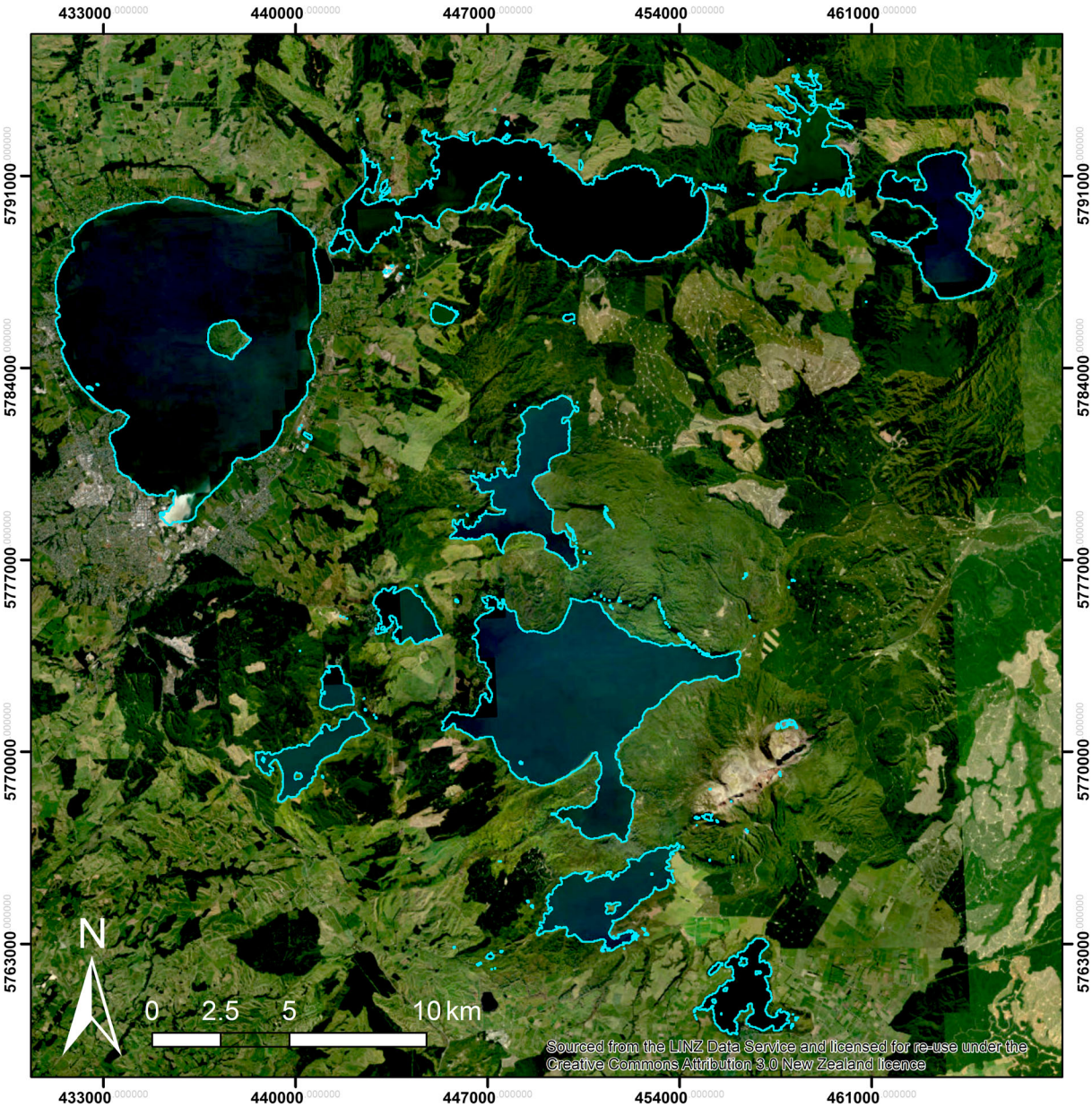

Fig. 3 Water boundaries derived from the automatic classification method. Lakes smaller than 1 ha were filtered in the later stage

Water index calculation and Google Earth Engine

$AWEI_{shadow}$ is optimized for the use when shadows result in a great reduction in accuracy and this index enhances the separation of water pixels from non-water sources. Detailed descriptions of formulation and equations can be found in Feyisa et al. (2014). In brief, an equation was developed to eliminate non-water pixels and then extract surface water by removing shadow pixels to further improve accuracy. This equation uses the reflectance values of five spectral bands of Landsat: band 1 (blue), band 2 (green), band 4 (NIR), band 5 (SWIR), and band 7 (SWIR), with the coefficients based on an empirical dataset of pure pixels varying in land cover.

$$AWEI_{shadow} = \rho_{band1} + 2.5 \times \rho_{band2} - 1.5 \times (\rho_{band4} + \rho_{band5}) - 0.25 \times \rho_{band7} \quad (1)$$

In which ρ is the reflectance values of Landsat 8 OLI.

GGE is then used to extract water surfaces for the whole of New Zealand. For large-scale and long-term applications of GEE, large amounts of data could be processed directly on the platform without downloading to the local computers, which did not require computational sources on local computers (Tang et al. 2016). Such characteristics allow examining images and changes over time and performing geospatial analysis much faster. The processing and data analysis steps were first run in GEE and included (1) choosing Landsat images with the cloud cover less than 10%, (2) deriving $AWEI_{shadow}$ raster images using the formula (1) by calculating $AWEI_{shadow}$ with the Earth Engine API (in JavaScript), (3) filtering water pixels which had the $AWEI_{shadow}$ values higher than zero, and (4) converting water polygons in KML format derived from GEE outcomes to shapefile format in ArcGIS. In ArcGIS, the GEE water polygons output was overlain over the study period to calculate water surface changes. In addition, accuracy assessment was also calculated with geospatial tools in ArcGIS.

Accuracy assessment

We only considered lakes larger than 1 ha because according to Olmanson et al. (2011) the smallest pixel size of inland water bodies could be seen from space by Landsat was 1 ha (100 m × 100 m). Overall accuracy (also called overall agreement, OA), producer's accuracy (PA), and Kappa (κ) indices were used to measure the accuracy of classification maps. As in Cohen (1960), Kappa is defined as follows:

$$\kappa = \frac{p_o - p_e}{1 - p_e} \quad (2)$$

$$p_e = \frac{1}{N^2 \sum_k n_{k1} n_{k2}} \quad (3)$$

where p_o is called the relative observed agreement, p_e is the hypothetical probability of chance agreement, N is the number of items, n_{ki} is the number of times rater i predicted category k.

The classification results were compared with ground-truth data collected at 1416 points in both the North and South Islands using GPS during field surveys in the years 2016–2017. Water boundaries derived from this automatic framework were also compared with water boundaries derived from the manual method based on aerial photos with 0.5 m resolution available at https://data.linz.govt.nz/. (LINZ.NZ).

Results

Model validation

Automatic water surface extraction with GEE and AWEI with lakes larger than 1 ha exhibited an overall good agreement between water pixels derived from this framework and ground surveys (Figs. 1 and 3). Table 1 shows the accuracy assessment for this automatic water extraction framework with Landsat 8 OLI and AWEI index. Acceptable values of PA and OA indices (> 80%; Table 1) allowed the application of this framework in classifying water for large-scale management.

Table 1 Accuracy assessment for automatic water extraction with GEE and AWEI

Class	References		UA (%)
	Water	Non-water	
Water	1200	216	84.7
Non-water	250	1469	85.5
PA (%)	82.8	87.2	
OA (%)	85.1		
Kappa	0.7		

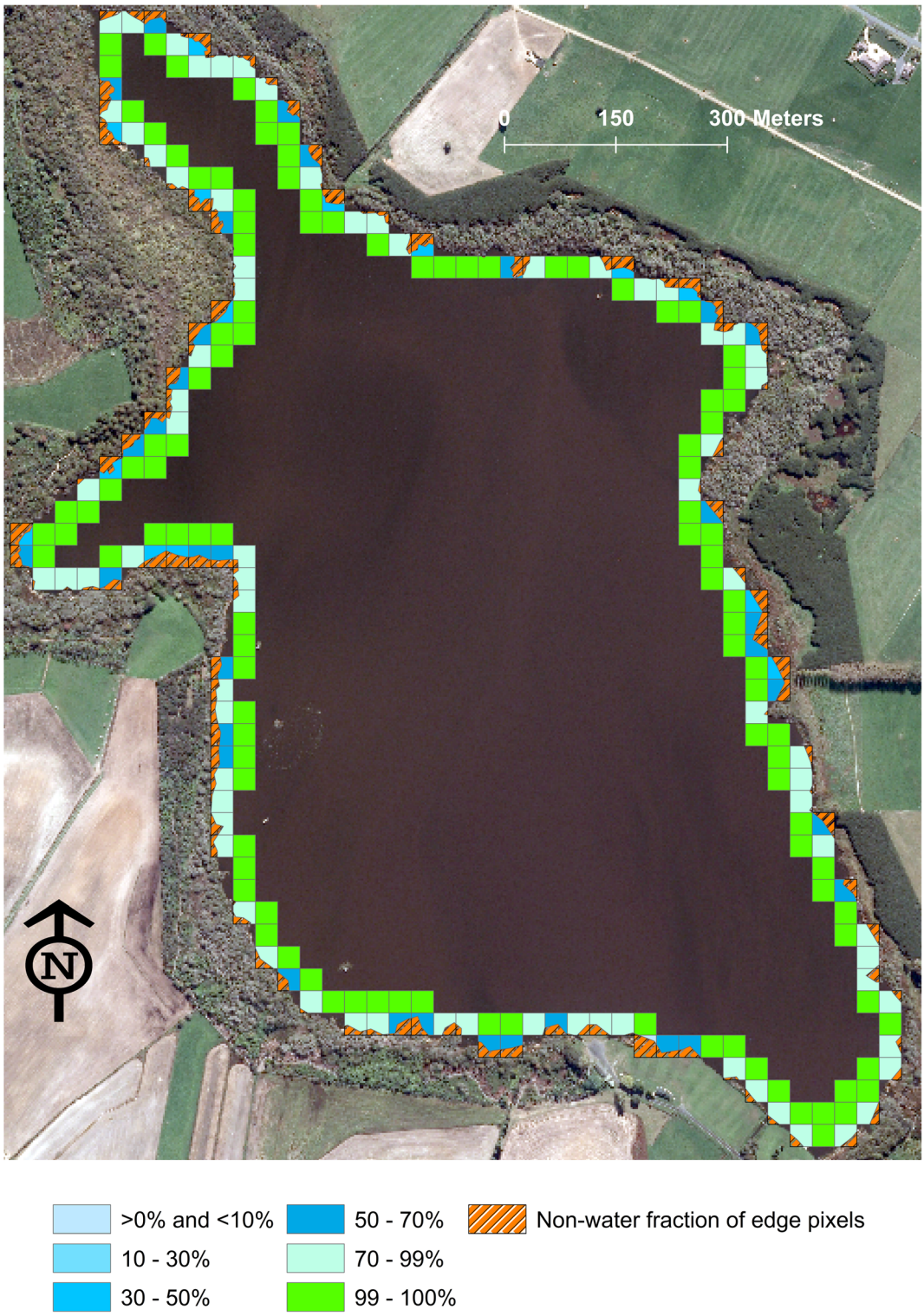

Fig. 4 Visual comparison between water boundaries derived from automated and manual methods (blue colors show the percentage of water fraction of each edge pixel when yellow color with strips is non-water fraction of edge pixels)

In Feyisa et al. (2014), the Kappa coefficient for lakes ranged between 0.93 and 0.98 which was higher than the Kappa value in this study ($\kappa = 0.7$). This may originate from the samples in our study which were taken from various sizes of lakes and at the edge of lakes. If samples were taken in the center of large lakes, there was a low probability that water pixels were misclassified.

Relating to the size of lakes, a misinterpretation of pixels was found for small lakes or reservoirs. This may be a result of the coarse Landsat pixel resolution (compared to the size of small lakes), which caused mixed pixels of water bodies and other forms of land use. Figure 4 shows the difference in edge pixels around Lake Ngaroto derived from this automatic water boundary detection method and the visual interpretation method using the aerial photos. The boundary derived from the automatic method was coarser than the manual method with high-resolution images. However, with this automatic method, the non-water fraction of edge water could be negligible if comparing the spatial resolutions of Landsat 8 (30 m) and the aerial photos (0.5 m). For large lakes, the differences were minor. Even with different types of lakes (e.g., shallow lake, deep lake, or volcanic lake), water depth and water color did not influence the results of this method. The high-spatial resolution of satellite images would allow us to better separate water pixels from other types of land use.

Spatial distribution of lakes

Although Landsat 8 OLI was equipped with sophisticated and modern sensors for earth observation, it did not have the cloud penetration capacity. Landsat 8 OLI flyovers occurred on average of 10 times per years for the period 2013–2017, and the total number of observations were less than 800. The number of lakes detected by the remote sensing method and most recent national field surveys (Leathwick et al. 2010) were similar (Fig. 5a; at above 3800 lakes) for the number of lakes and reservoirs with open water. A total area of 3742 km^2 water surface was detected with around two-thirds of the lakes in the southern part of the country. The lakes were evenly distributed throughout the country, but large lakes could be found more in the mountainous areas of the South Island. However, shallow lakes and those with a small footprint might be under reported.

Seasonal and inter-annual variability

Special inter-annual or intra-annual changes in water boundaries of lakes and reservoirs during the study period were not detected (Fig. 6). This may be because of a result of the study period being short (i.e., Landsat 8 was launched in 2013). Also of

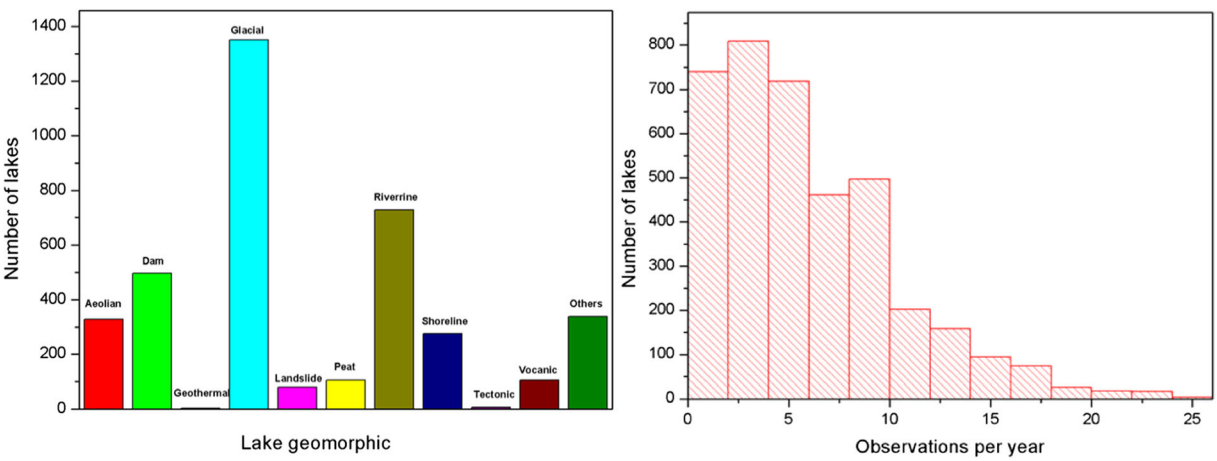

Fig. 5 **a** Number of lakes and their relative distributions according to field surveys, showing a dominated number of glacial lakes compared to other types; **b** frequency lake observation per year from Landsat 8 OLI; cloud coverage is the main reason of the number of observations per year below 10

interest is that the AWEI index could not distinguish between different forms of water (liquid, ice, or snow). Therefore, lakes, especially in mountainous areas or southern parts of the country, could not be detected in the winter (from June to August; e.g., Lake Tekapo in the North Island, Fig. 6). Although a 10% of cloud coverage was chosen as a threshold to select images, data anomaly was detected in several photos (Fig. 6; Lake Tarawera May 2015; Lake Tekapo Feb 2015; Rotorua Mar 2016).

Discussion

The combination of AWEI and GEE resulted in a fast and robust framework for automatic water body recognition. This combination reduced the burden of manual classification, and it increased productivity, accuracy, and quality for macro water resource monitoring and assessment. The AWEI index showed its capability of distinguishing different types of lakes from other land cover types with the OA of 0.85. However, this index

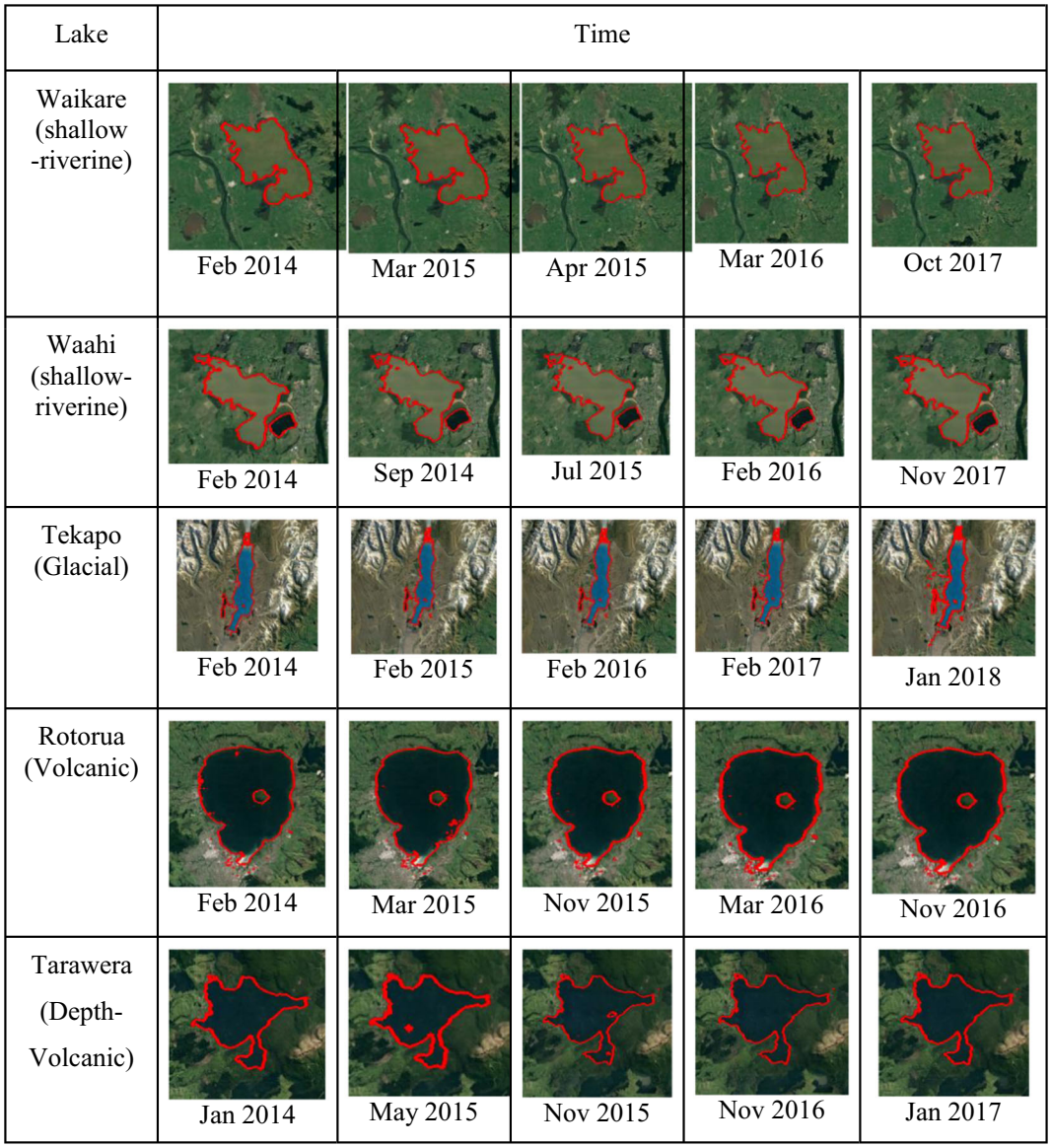

Fig. 6 Water boundaries over years of sakes with different characteristics in New Zealand. The areas of Waikare, Waahi, Tekapo, Rotorua, and Tarawera did not change over the study period, and it was impossible to estimate the areas of Tekapo (glacial lake) during the winter

should be used with care in snowy or icy regions. The limitation of the equations was also shown in classifying high albedo surfaces as in (Feyisa et al. 2014).

In terms of spatial distributions of lakes in New Zealand, there were around 3840 lakes and reservoirs larger than 1 ha. This was much greater than 775 lakes with lengths of 0.5 km as reported in Lowe and Green (1992). The difference, however, may originate from the thresholds (0.5 km and 1 ha).

Overall, there was no trend in the total areas of water surfaces (Fig. 6) in New Zealand's lakes for the time of this study, despite global climatic variation. The monthly average values of multivariate El Niño-Southern Oscillation Index (MEI) (suggested by Wolter and Timlin 1998) for New Zealand from 2013 to 2017 and monthly average rainfall from 2013 to 2015 for the whole New Zealand are shown in Fig. 7. The period from January 2015 to July 2016 was possibly a strong El Niño period (Fig. 7), and rainfall reached its maximum amount in August 2015 (219.2 mm) when the ENSO index was 2.368. This value was much higher than rainfall intensity values in August 2013 (137.81 mm) and August 2014 (117.18 mm). Nevertheless, remote sensing data analysis showed that areal surfaces of lakes and reservoirs were not different over the study period. It is also worth to mention that although satellite data was highly reliable, the spatial resolution of Landsat 8 OLI was 30 m which might be sometimes too coarse to detect changes in surface areas if lake banks were steep.

Climate change and human disturbance have changed hydrological regimes worldwide. While the impact of human activities on hydrological regimes become larger than climate change impacts, climate variability will still be dominate in higher latitude and altitude areas (Gleick 1989). As a result, climate change will increase the pressure on water flows around the world (Gleick 1989; Christensen et al. 2004; Dang et al. 2018a). Since the influence of both drivers on the hydrological cycle is ongoing, the application of an automatic monitoring framework as provided in this study will contribute significantly to conservation programs.

There were several uncertainties related to this study. Although the Landsat 8 OLI satellite has captured the earth's surface with a regular interval of 16 days, the number of images acquired for each lake was almost less than ten times (Fig. 5b). This problem was dependent on the local density of cloud coverage. Secondly, the spatial resolution of Landsat reduced the accuracy of the classification results for small lakes because of the mixture of water pixels and other types of land cover (Fig. 4). Therefore, future research needs to have higher spatial resolution satellite images to minimize the problem of mixed pixels. Moreover, the integration of optical remote sensing derived from frequent-return satellite data with high-spatial resolution sensors, ground-truth, and in situ data have the potential to improve accuracy assessment and ultimately increase the predictive power for monitoring management tools (Nguyen 2015). Another suggestion is using drones or unnamed aerial vehicle systems (UAVs) for several small lakes that may not have been identified by satellite, due to limited access or cloud cover and other atmospheric influences.

Conclusion

This paper proved that the application of AWEI and Landsat could be useful in water surface monitoring

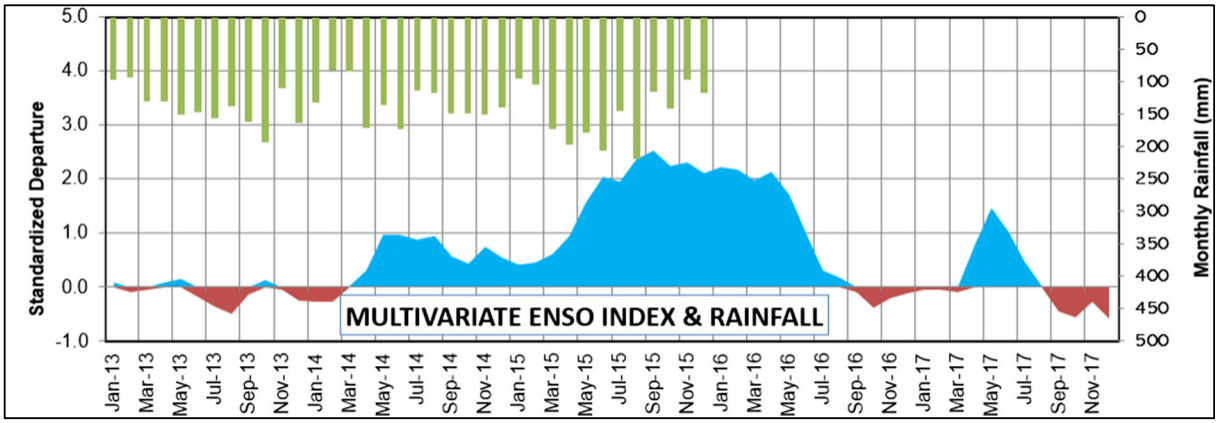

Fig. 7 Multivariate ENSO index (MEI) for New Zealand in monthly, so the actual value shows the mean of 2 months (Source: NOAA)

on the Google Earth Engine platform except for snowy or icy regions. In the context of the current global water crisis, further studies which analyze the variation of water surface dynamics in a longer period and simulate the impact of future climate change on water availability are required. The framework implemented in this study can be applied for water quality monitoring by combining with in situ data and spatial interpolation as in Dang et al. (2018a). Therefore, it may then support stakeholders and policy makers to improve water quantity control and sustainable water management. Future works can also consider object-based segmentation methods combined with AWEI and GEE to enhance the accuracy of water extraction. This technique will benefit both water resource monitoring and management and provide a vital framework with broad applicability for ecosystem service values.

This study exhibited that intra- and inter-annual water surface areas in most of the lakes in New Zealand did not change over the study period. However, the spatial resolution of Landsat and cloud coverage could reduce the level of accuracy. Therefore, finer resolution satellite products should be considered to further investigate changes in lake areas.

Acknowledgements We wish to thank the editor in handling this paper, and we also acknowledge the anonymous reviewers for their great comments and edits which helped us to improve the quality of this paper significantly.

References

Bai, J., Chen, X., Li, J., Yang, L., & Fang, H. (2011). Changes in the area of inland lakes in arid regions of central Asia during the past 30 years. *Environmental Monitoring and Assessment, 178*(1–4), 247–256.

Cann, K. F., Thomas, D. R., Salmon, R. L., Wyn-Jones, A. P., & Kay, D. (2013). Extreme water-related weather events and waterborne disease. *Epidemiology & Infection, 141*(4), 671–686.

Christensen, N. S., Wood, A. W., Voisin, N., Lettenmaier, D. P., & Palmer, R. N. (2004). The effects of climate change on the hydrology and water resources of the Colorado River basin. *Climatic Change, 62*(1–3), 337–363.

Cohen, J. (1960). A coefficient of agreement for nominal scale. *Educational and Psychological Measurement, 20*, 37–46.

Danaher, T., & Collett, L. (2006). *Development, optimization and multi-temporal application of a simple Landsat based water index*. The 13th Australasian Remote Sensing and Photogrammetry Conference. Canberra.

Dang, T. D., Cochrane, T. A., Arias, M. E., Van, P. D. T., & de Vries, T. T. (2016). Hydrological alterations from water infrastructure development in the Mekong floodplains. *Hydrological Processes, 30*(21), 3824–3838.

Dang, T. D., Cochrane, T. A., Arias, M. E., & Van, P. D. T. (2018a). Future hydrological alterations in the Mekong Delta under the impact of water resources development, land subsidence and sea level rise. *Journal of Hydrology: Regional Studies, 15*, 119–133.

Dang, T. D., Cochrane, T. A., & Arias, M. E. (2018b). Quantifying suspended sediment dynamics in mega deltas using remote sensing data: a case study of the Mekong floodplains. *International Journal of Applied Earth Observation and Geoinformation, 68*, 105–115.

Donchyts, G., Schellekens, J., Winsemius, H., Eisemann, E., & van de Giesen, N. (2016). A 30 m resolution surface water mask including estimation of positional and thematic differences using landsat 8, srtm and openstreetmap: a case study in the Murray-Darling Basin, Australia. *Remote Sensing, 8*(5), 386.

Duan, Z., & Bastiaanssen, W. (2013). Estimating water volume variations in lakes and reservoirs from four operational satellite altimetry databases and satellite imagery data. *Remote Sensing of Environment, 134*, 403–416.

Feng, M., Sexton, J. O., Channan, S., & Townshend, J. R. (2016). A global, high-resolution (30-m) inland water body dataset for 2000: first results of a topographic–spectral classification algorithm. *International Journal of Digital Earth, 9*(2), 113–133.

Feyisa, G. L., Meilby, H., Fensholt, R., & Proud, S. R. (2014). Automated Water Extraction Index: a new technique for surface water mapping using Landsat imagery. *Remote Sensing of Environment, 140*, 23–35.

Fisher, A., Flood, N., & Danaher, T. (2016). Comparing Landsat water index methods for automated water classification in eastern Australia. *Remote Sensing of Environment, 175*, 167–182.

Gao, Y., Riklin-Raviv, T., & Bouix, S. (2014). Shape analysis, a field in need of careful validation. *Human Brain Mapping, 35*(10), 4965–4978. https://doi.org/10.1002/hbm.22525.

Giardino, C., Bresciani, M., Villa, P., & Martinelli, A. (2010). Application of remote sensing in water resource management: the case study of Lake Trasimeno, Italy. *Water Resources Management, 24*, 3885–3899.

Gleick, P. H. (1989). Climate change, hydrology, and water resources. *Reviews of Geophysics, 27*(3), 329–344.

Gorelick, N., Hancher, M., Dixon, M., Ilyushchenko, S., Thau, D., & Moore, R. (2017). Google Earth Engine: planetary-scale geospatial analysis for everyone. *Remote Sensing of Environment, 202*, 18–27.

Güttler, F. N., Niculescu, S., & Gohin, F. (2013). Turbidity retrieval and monitoring of Danube Delta waters using multi-sensor optical remote sensing data: an integrated view from the delta plain lakes to the western–northwestern Black Sea coastal zone. *Remote Sensing of Environment, 132*, 86–101.

Hui, F., Xu, B., Huang, H., Yu, Q., & Gong, P. (2008). Modelling spatial-temporal change of Poyang Lake using multitemporal Landsat imagery. *International Journal of Remote Sensing, 29*, 5767–5784.

Ji, L., Zhang, L., & Wylie, B. (2009). Analysis of dynamic thresholds for the normalized difference water index.

Photogrammetric Engineering & Remote Sensing, 75, 1307–1317.

Leathwick, J. R., West, D., Gerbeaux, P., Kelly, D., Robertson, H., Bronwn, D., Chadderton, W. L., & Ausseil, A.-G. (2010). *Freshwater ecosystems of New Zealand (FENZ) geodatabase version one - user guide*. Wellington: NIWA.

Li, W., Du, Z., Ling, F., Zhou, D., Wang, H., Gui, Y., Sun, B., & Zhang, X. (2013). A comparison of land surface water mapping using the normalized difference water index from TM, ETM+ and ALI. *Remote Sensing, 5*, 5530–5549.

LINZ. NZ *Aerial Imagery. Sourced from the LINZ Data Service* (https://data.linz.govt.nz/) and licensed by the copyright holder for re-use under the Creative Commons Attribution 3.0 New Zealand. Accessed 15 Jan 2018

Lowe, D. J., & Green, J. D. (1992). Lakes. In J. M. Soons & M. J. Selby (Eds.), *Landforms of New Zealand* (2nd ed., p. 108). Auckland: Longman Paul.

Lymburner, L., Botha, E., Hestir, E., Anstee, J., Sagar, S., Dekker, A., & Malthus, T. (2016). Landsat 8: providing continuity and increased precision for measuring multi-decadal time series of total suspended matter. *Remote Sensing of Environment, 185*, 108–118.

McCullough, I. M., Loftin, C. S., & Sader, S. A. (2013). Lakes without Landsat? An alternative approach to remote lake monitoring with MODIS 250 m imagery. *Lake and Reservoir Management, 29*(2), 89–98.

Mcfeeters, S. K. (1996). The use of the Normalized Difference Water Index (NDWI) in the delineation of open water features. *International Journal of Remote Sensing, 17*, 1425–1432.

New Zealand statistics. (2006). *New Zealand in profile* (p. 30). Wellington: Statistics New Zealand.

Nguyen, U. (2015). *Multiscale remote sensing analysis to monitor riparian and upland semi-arid vegetation*. PhD Dissertation, University of Arizona, Tucson, Arizona.

Nguyen, U., Glenn, E. P., Nagler, P. L., & Scott, R. L. (2015). Long-term decrease in satellite vegetation indices in response to environmental variables in an iconic desert riparian ecosystem: The Upper San Pedro, Arizona, United States. *Ecohydrol., 8*, 608–623.

Nguyen, U., Glenn, E. P., Dang, T. D., & Pham, L. T. (2019). Mapping vegetation types in semi-arid riparian regions using random forest and object-based image approach: a case study of the Colorado River Ecosystem, Grand Canyon, Arizona. *Ecological Informatics, 50*, 43–50.

Olmanson, L. G., Brezonik, P. L., & Bauer, M. E. (2011). Evaluation of medium to low resolution satellite imagery for regional lake water quality assessments. *Water Resources Research, 47*, 1–14.

Ouma, Y. O., & Tateishi, R. (2006). A water index for rapid mapping of shoreline changes of five East African Rift Valley lakes: an empirical analysis using Landsat TM and ETM+ data. *International Journal of Remote Sensing, 27*, 3153–3181.

Pham, L. T., & Brabyn, L. (2017). Monitoring mangrove biomass change in Vietnam using SPOT images and an object-based approach combined with machine learning algorithms. *ISPRS Journal of Photogrammetry and Remote Sensing, 128*, 86–97.

Pham, L. T., Vo, T. Q., Dang, T. D., & Nguyen, U. T. (2019). Monitoring mangrove association changes in the Can Gio biosphere reserve and implications for management. *Remote Sensing Applications: Society and Environment, 13*, 298–305.

Prigent, C., Papa, F., Aires, F., Jimenez, C., Rossow, W., & Matthews, E. (2012). Changes in land surface water dynamics since the 1990s and relation to population pressure. *Geophysical Research Letters, 39*(8), L08403, 1–5.

Proud, S. R., Fensholt, R., Rasmussen, L. V., & Sandholt, I. (2011). Rapid response flood detection using the MSG geostationary satellite. *International Journal of Applied Earth Observation and Geoinformation, 13*, 536–544.

Qiao, C., Luo, J., Sheng, Y., Shen, Z., Zhu, Z., & Ming, D. (2012). An adaptive water extraction method from remote sensing image based on NDWI. *Journal of the Indian Society of Remote Sensing, 40*, 421–433.

Shelestov, A., Lavreniuk, M., Kussul, N., Novikov, A., & Skakun, S. (2017). Large scale crop classification using Google earth engine platform. In *Geoscience and Remote Sensing Symposium (IGARSS), 2017 IEEE International* (pp. 3696–3699). IEEE.

Sun, F., Sun, W., Chen, J., & Gong, P. (2012). Comparison and improvement of methods for identifying waterbodies in remotely sensed imagery. *International Journal of Remote Sensing, 33*, 6854–6875.

Tang, Z., Li, Y., Gu, Y., Jiang, W., Xue, Y., Hu, Q., & Li, R. (2016). Assessing Nebraska playa wetland inundation status during 1985–2015 using Landsat data and Google Earth Engine. *Environmental Monitoring and Assessment, 188*(12), 654.

Verpoorter, C., Kutser, T., & Tranvik, L. (2012). Automated mapping of water bodies using Landsat multispectral data. *Limnology and Oceanography: Methods, 10*, 1037–1050.

Wolter, K., & Timlin, M. S. (1998). Measuring the strength of ENSO - how does 1997/98 rank? *Weather, 53*, 315–324.

Wood, E. F., Roundy, J. K., Troy, T. J., Van Beek, L. P. H., Bierkens, M. F., Blyth, E., et al. (2011). Hyperresolution global land surface modeling: meeting a grand challenge for monitoring Earth's terrestrial water. *Water Resources Research, 47*(5), W05301, 1–10.

Xu, H. (2006). Modification of normalised difference water index (NDWI) to enhance open water features in remotely sensed imagery. *International Journal of Remote Sensing, 27*, 3025–3033.

Publisher's note Springer Nature remains neutral with regard to jurisdictional claims in published maps and institutional affiliations.